TECTONICS, VOL. 32, 19–33, doi:10.1029/2012TC003189, 2013

Recent, slow normal and strike-slip faulting in the Pasto Ventura region of the southern Puna Plateau, NW Argentina

Renjie Zhou,[1,2] Lindsay M. Schoenbohm,[1,2] and Michael Cosca[3]

Received 28 June 2012; revised 5 November 2012; accepted 20 November 2012; published 28 January 2013.

[1] Recent normal and strike-slip faulting on the Puna Plateau of NW Argentina has been linked to lithospheric foundering, gravitational spreading, plate boundary forces and a decrease in crustal shortening from north to south. However, the timing, kinematics and rate of extension remain poorly constrained. We focus on the Pasto Ventura region (NW Argentina) located on the southern Puna Plateau and recent deformation (<1 Ma). Field mapping and kinematic analysis across offset volcanic cinder cones show that the overall extension direction is subhorizontal, is oriented NE-SW to NNE-SSW, and occurs at a slow, time-integrated rate of 0.02 to 0.08 mm/yr since at least 0.8–0.5 Ma. A regional compilation from this study and existing data shows that recent extension across the Puna Plateau is subhorizontal but varies in azimuthal orientation dramatically. Data from the Pasto Ventura region are consistent with a number of models to explain normal and strike-slip faulting on the Puna Plateau, all of which likely influence the region. Some role for lower lithospheric foundering through dripping appears to be seen based on the regional extension directions and ages of mafic volcanism in the southern Puna Plateau.

Citation: Zhou R., L. M. Schoenbohm, and M. Cosca (2013) Recent, slow normal and strike-slip faulting in the Pasto Ventura region of the southern Puna Plateau, NW Argentina, *Tectonics*, *32*, 19–33, doi:10.1029/2012TC003189.

1. Introduction

[2] Horizontal extension of the Central Andean Plateau since the late Miocene is evident by strike-slip and normal faulting and is a consequence of a significant shift from vertical extension to vertical contraction of the Central Andean Plateau [*Allmendinger*, 1986; *Allmendinger et al*., 1989; *Marrett and Emerman*, 1992; *Mercier et al*., 1992; *Cladouhos et al*., 1994; *Kay et al*., 1994; *Marrett et al*., 1994; *Allmendinger et al*., 1997; *Riller and Oncken*, 2003; *Baldwin*, 2005; *Schoenbohm and Strecker*, 2009; *Montero Lopez, et al*., 2010; *Santimano and Riller*, 2012]. Horizontal extension, in spite of ongoing convergence, is common within other continental plateaus as well, such as in Tibet and Anatolia, and the origin is under debate. For regions with high mean elevation, it could be the result of gravitational spreading, in which extension is driven by the excess gravitational potential energy from the highly elevated crust, which overcomes the supporting stress from plate convergence [*Burchfiel and Royden*, 1985; *England and Houseman*, 1989; *Rey et al*., 2001; *Schoenbohm and Strecker*, 2009]. Extension in the Andes could reflect the dynamic forces of plate convergence, similar to Tibet in which normal faults are linked to the stress field produced by the indenting Indian plate [*Kapp and Guynn*, 2004]. This is an important model for the Tibetan Plateau, where N-S trending graben systems reflect E-W extension. Orogen-parallel extension, concurrent with orogen-perpendicular shortening, has been inferred for the Puna Plateau based on the rhomb-shaped geometry of Miocene and Pliocene crustal blocks, and attributed to plan view simple shear deformation related to a decrease in the degree of plateau shortening from north to south [*Riller and Oncken*, 2003; *Riller et al*., 2012]. Another possible cause of horizontal extension in the Puna Plateau, supported by observations of a thin crust and lithosphere (currently the thinnest crust and lithosphere is located beneath the Arizaro basin) [*Yuan et al*., 2002; *Tassara et al*., 2006], intraplate mafic arc volcanism [*Kay and Kay*, 1993; *Kay et al*., 1994] and recent normal faulting associated with mafic volcanism [*Kay et al*., 1994; *Allmendinger et al*., 1997; *Schoenbohm and Strecker*, 2009] is thermal and isostatic uplift in response to lithospheric foundering [e.g., *Kay et al*., 1994; *Babeyko and Sobolev*, 2005; *Oncken et al*., 2006].

[3] Before any model can be properly evaluated, however, detailed documentation of normal and strike-slip faulting, especially the rate, needs to be obtained first in order to understand potential causes of such deformation. In this study, we focus on the most recent (< 1 Ma) characteristics in the Pasto Ventura region on the southern plateau margin. By completing a detailed geomorphic-geological map in the Pasto Ventura region, we are able to identify normal and strike-slip faults developed mostly during Quaternary time.

[1]Department of Chemical and Physical Sciences, University of Toronto Mississauga, Mississauga, Ontario, Canada.
[2]Department of Earth Sciences, University of Toronto, Toronto, Ontario, Canada.
[3]Central Mineral and Environmental Resources Science Center, U.S. Geological Survey, Denver, Colorado, USA.

Corresponding author: R. Zhou, Department of Earth Sciences, University of Toronto, 22 Russell St., Toronto, ON M5S 3B1, Canada. (zhou@es.utoronto.ca)

0278-7407/12/2012TC003189

The faults cut Quaternary geomorphic features, and although they are characterized by a small degree of offset, they represent an important component of the most recent structural development of this region. We also map two older faults, reactivated in a normal sense, which cut several cinder cones and associated lava flows. To determine the net slip and slip rate of the normal faulting, we measure the offset using kinematic GPS surveying, date the offset volcanic features using $^{40}Ar/^{39}Ar$ geochronology and perform geometric analysis. We find that the extension rate is extremely slow. We also discuss how our data fit with a number of proposed mechanisms for producing horizontal extension on the Puna Plateau.

2. Background

[4] The Central Andean Plateau is the world's second largest continental plateau, and is located on a noncollisional plate boundary (Figure 1). Its area can be approximately defined by the 3000 m elevation contour, and it is largely internally drained [*Allmendinger et al*., 1997, and references therein]. The formation of the Central Andean Plateau is related to eastward subduction of the Nazca Plate nearly orthogonally to the South America Plate boundary at a rate of 50–150 mm/yr since about 50 Ma [*Pardo-Casas and Molnar*, 1987; *Somoza*, 1998; *Marrett and Strecker*, 2000]. The plateau stretches 1500 km along the western edge of the South American continent and is 300–500 km in width. The Central Andean Plateau is curved at ~20°S, where the plateau trend changes from NNE-SSW in the Puna to the south to NW-SE in the Altiplano to the north. The current surface topography in the Puna Plateau is strikingly different from that in the Altiplano. As illustrated by the distribution of areas that have a less than 2° surface slope, the center of the Altiplano Plateau is dominated by one large, central basin, whereas the Puna Plateau is characterized by more rugged topography and smaller, intervening basins (Figure 1). The largest geomorphic basins on the Puna Plateau include the Arizaro, Antofalla, Antofagasta, Pasto Grandes and Pasto Ventura regions (Figures 1 and 2).

[5] The plateau region has experienced a complex geological history. Convergence during the Cenozoic [*Mpodozis et al*., 2005; *Arriagada et al*., 2006; *Carrapa and DeCelles*, 2008] built the Central Andean Plateau through a variety of proposed mechanisms, including distributed crustal shortening [*Allmendinger et al*., 1997, and references therein], megathrust of basement rocks [*McQuarrie*, 2002], and cratonic under thrusting [*Cladouhos et al*., 1994; *McCaffrey and Nabelek*, 1998]. The Central Andean Plateau is underlain by relatively thick crust (>50 km). However, geophysical data suggest thinner crust and mantle lithosphere beneath the Puna Plateau in the south compared to the Altiplano Plateau in the north. P and S receiver function and wide-angle reflection studies reveal that the crustal thickness in the Puna is 50–68 km [*Yuan et al*., 2002; *McGlashan et al*., 2008]. Beneath the Salar de Arizaro of the northern Puna Plateau, gravity modeling indicates that the mantle lithosphere may be totally absent (Figures 1 and 2) [*Tassara et al*., 2006].

[6] Magmatism on the Puna Plateau is mainly composed of shoshonitic lavas, intraplate and calc-alkaline lavas and voluminous ignimbrites, most of which are late Miocene and younger [e.g., *de Silva*, 1989; *Coira and Kay*, 1993; *Kay and Coira*, 2009]. Small-volume, mafic lavas have erupted on the Puna Plateau since 7.3 Ma [*Risse et al*., 2008]: intraplate-like lavas are concentrated in the center of the southern

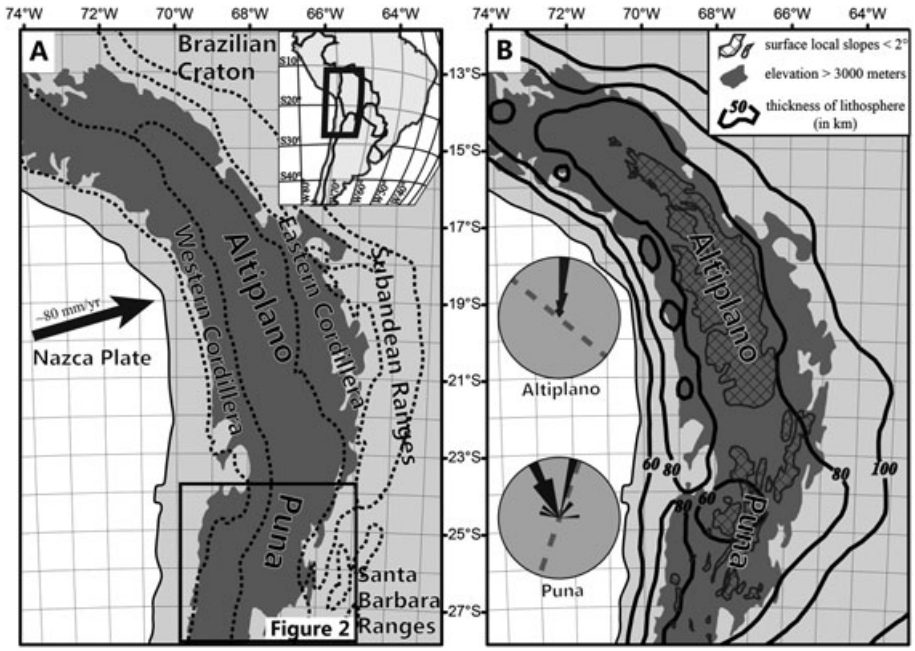

Figure 1. Overview map of the Andes. (a) Tectonic divisions of the Andes [after *Schoenbohm and Strecker*, 2009]. Black arrow shows the vector for Nazca Plate [*Marrett and Strecker*, 2000]. Box marks the location of Figure 2. (b) Contours of lithospheric thickness [after *Tassara et al*., 2006] and location of basins within the Altiplano and Puna Plateaus. Rose diagrams show extension directions within the plateau [after *Schoenbohm and Strecker*, 2009], in which the dashed lines show the trend of the Altiplano Plateau (north) and the Puna Plateau (south).

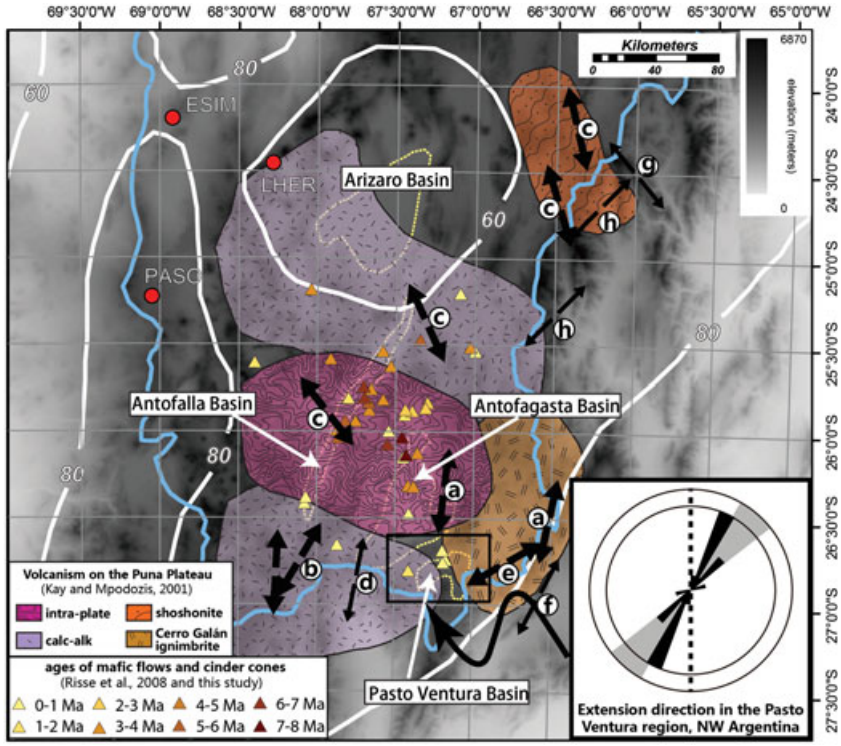

Figure 2. Summary map of morphology, volcanism and extension on the Puna Plateau. White lines are contours for lithosphere thickness [from *Tassara et al*., 2006]. Fields for volcanism are from *Kay* and *Mpodozis*, [2001]. Age data for mafic volcanism (triangles) are from *Risse et al*. [2008] and this study. Note clustering of older volcanoes around 26°S. Red dots are GPS stations from SAGA [*Khazaradze and Klotz*, 2003]. Horizontal extension directions (double arrows) are from the following sources: a, *Allmendinger* [1986] and *Allmendinger et al*. [1989]; b, *Baldwin* [2005]; c, *Marrett et al*. [1994]; d, *Montero Lopez et al*. [2010]; e, *Schoenbohm and Strecker* [2009]; f, *de Urreiztieta et al*. [1996]; g, *Marrett and Strecker* [2000]; h, *Santimano and Riller* [2012]. Blue line outlines the plateau margin based on the 3000 m elevation contour. The bold arrows denote the extension directions on the plateau while the thin arrows denote those off the plateau. Yellow dashed lines are locations of current geomorphic basins on the Puna Plateau. Inset shows the extension direction in the Pasto Ventura Basin as determined in this study. Outer circle indicates extension direction constrained by vertical and horizontal offsets across Fault PV02. Inner circle is rose diagram for the extension directions revealed by 13 Group 1 Quaternary faults (normal faults only) (Table 1). Black box shows location of Figure 3.

Puna Plateau, with arc-like magmatism to the north and south (Figure 2) [*Kay et al*., 1994, 1999]. Some of the volcanism is linked to the evolution of several major NW-SE trending lineaments: the deep-seated and long-lived basement structures or anisotropies that cross the Andes [e.g., *Schreiber and Schwab*, 1991; *Richards and Villeneuve*, 2002; *Petrinovic et al*., 2005]. Volcanism has also been interpreted to reflect the generation of magmas through the influx of hot asthenosphere, as the lower lithosphere was removed during mid-late Miocene [*Kay and Kay*, 1993; *Kay et al*., 1994]. Geochemical investigations demonstrate high K concentrations and La/Ta ratios of <25 for the intraplate lavas, suggesting they originated from a highly modified source [*Kay et al*., 1994]. Further, the eruption of the Cerro Galán ignimbrite, as well as other ignimbrites to the north could have occurred as mantle-derived basaltic melt entered and melted the crust, producing hybrid melts that evolved into the felsic magmas [*Kay and Coira*, 2009; *Kay et al*., 2009, 2010]. Miocene flat slab subduction in the Puna could have been responsible for the eruption of some of the ignimbritic material, because a hydrated flat slab would act as a flux for melting the crust and mantle lithosphere and "precondition" the mantle lithosphere for foundering [e.g., *Humphreys*, 2009].

[7] Despite ongoing plate convergence, widespread recent horizontal extension within the plateau has been widely recognized [*Allmendinger et al*., 1989; *Mercier et al*., 1992; *Cladouhos et al*., 1994; *Marrett et al*., 1994; *Allmendinger et al*., 1997; *Riller et al*., 2001; *Riller and Oncken*, 2003; *Schoenbohm and Strecker*, 2009; *Montero Lopez et al*., 2010]. Horizontal extension may have begun as early as circa 10 Ma, based on the eruption age of a collapse caldera in the Puna Plateau [*Riller et al*., 2001]. Other studies suggest a slightly younger age of initiation based on the eruption of basaltic magmas beginning at 7.3 Ma [e.g., *Risse et al*., 2008], as the dense mafic material would not be able to travel through the crust under contractional conditions [*Marrett and Emerman*, 1992]. Another study focused on the structural relationship of offset rock units concludes that regional extension in the Puna was already well established by 5 Ma and could have begun earlier [*Montero Lopez et al*., 2010]. This phase of extension on the plateau is characterized by normal and strike-slip faults that crosscut or reactivate preexisting reverse

and thrust faults [*Allmendinger et al*., 1997, and references therein; *Schoenbohm and Strecker*, 2009]. Extensional faulting has also been identified within four major transverse volcanic zones defined by NW-SE striking first-order fault systems, or lineaments, such as the Lipez, Olacapato–El Toro, Archibarca and Culampaja fault zones [e.g., *Riller et al*., 2001; *Acocella et al*., 2011]. Horizontal extension has been attributed to simple shear of the plateau in response to a southward decrease in crustal shortening [*Riller and Oncken*, 2003]. Such deformation would result in overall NNE-SSW horizontal extension, accommodated by orogen parallel (N-S) and orogen oblique (NE-SW) dominantly strike-slip faults defining rhomb-shaped subbasins [*Riller and Oncken*, 2003]. However, others argue that extension on the Puna Plateau is linked to lower lithospheric foundering [*Marrett and Emerman*, 1992; *Kay and Kay*, 1993; *Kay et al*., 1994; *Allmendinger et al*., 1997, and references therein; *Risse et al*., 2008].

3. Methods

3.1. Geomorphic and Geological Mapping

[8] One of our contributions in this paper is a detailed geomorphic-geological map of the Pasto Ventura region, NW Argentina (Figure 3), from ~26°40′S to 27°S, and ~67°5′W to 67°30′W. The map was created at a scale of approximately 1:50,000 and uses a 90 m resolution shaded relief map derived from SRTM (Shuttle Radar Topography Mission) DEM data as its base. Both field mapping and remote mapping with aerial photographs, satellite images and DEM data were used, with remote interpretations verified in the field. Vegetation on the Puna Plateau is mainly sparsely distributed short bush, allowing for high-precision image-based mapping. There are relatively few non-Quaternary units in the region, all easily identifiable in remote imagery by their unique textures and colors.

[9] The bedrock for the Pasto Ventura region is the Puncoviscana Formation which consists of clastic, weakly metamorphosed sedimentary rocks in this region [*Allmendinger et al*., 1997; *Ramos*, 2008, and references therein]. These are characterized in remote imagery by high topography and a fracture-rich, dark colored appearance. Although a number of Neogene sedimentary units have been identified in the map area, because our focus is on recent faulting, we refer to these strata as one unit for the purposes of our map. These are easily identifiable in remote imagery by the closely spaced, parallel lineaments which form prominent ridges and valleys. Mafic cinder cones and lava flows are also mapped. Lava flows have relatively high topography and clear flow structures on the surface, and are nearly black in color. Although the small-volume, monogenetic mafic volcanoes are as old as late Miocene (*Coira et al*. 1982, *Kay et al*. 1994], *Risse et al*. 2008], and data herein), given the low erosion rates on the plateau, the shape of the cinder cones has been preserved. Lava flows may or may not be associated with cinder cones and some of the cinder cones could have been buried underneath their associated lava flows. In the eastern part of the map, an area of andesitic basalt is exposed, partially covered by colluvial and eolian sediments. This unit is distinguished from mafic Quaternary lava flows by its lighter color. Additionally, these lavas have undergone more erosion, evidenced by lower topography and the lack of primary flow structures on the surface. Although there are no geochronologic data for this unit, we infer it predates recent, mafic volcanism.

[10] The majority of the map area is covered by unconsolidated sediments. We subdivide these into 6 Quaternary units (Figure 3). Colluvial sediments (Qc) are found in most of the map area, characterized by irregular, coarse clasts (fine materials have been removed by winnowing) and gentle to moderate slopes. There are two types of eolian sediments in our mapping area: Quaternary eolian sands (Qe) and Quaternary eolian volcanic clasts (Qbw). Qe is usually found on the lee of topography and/or faults. Qbw, on the other hand, is found immediately adjacent to basaltic cinder cones or flows and is shown by dark, high-density colors on the air photos. The region is cut by several river channels which are mapped as Quaternary alluvial channel sediments (Qa). These river channels are currently dry, and are blocked by large dunes in some cases. Quaternary terraces (Qt) are associated with the channels. Qt usually builds higher topography than the colluvial surface nearby and shows finer-grain sediments on the surface. Quaternary alluvial fan sediments (Qf) slope relatively steeply and can be traced directly to mountain sources. Field observation reveals that they are relatively finer grained than colluvial deposits. We also map out other geomorphic features on the surface such as sinter deposits (characterized by silica-cemented sediments, highly resistant to weathering, with a bright white color in remote imagery), modern salars and lakes.

[11] Such detailed examination of the Quaternary sediments enabled us to identify and map 13 normal and two strike-slip faults that offset river channels, colluvial surfaces, and terraces. We also mapped several large, previously identified normal faults which bound metamorphic bedrock and reactivate older, high-angle reverse faults [*Allmendinger et al*., 1989; *Marrett et al*., 1994; *Allmendinger et al*., 1997]. On the Puna Plateau, much of the landscape is covered with sand, loess or shattered rock debris, or desert pavement has formed. Thus fault plane exposures are rare and fault scarps are frequently buried by meters of debris. This inevitably causes difficulties in determining fault kinematics for studies based on field mapping, such as this one.

3.2. Kinematic GPS Survey

[12] Kinematic GPS survey systems, which provide subcentimeter level precision [*Cannon*, 1990], are a powerful tool used for high-precision topographic mapping [*Borsa et al*., 2008], and to measure fault offset [*Simoes et al*., 2007; *Lee et al*., 2009; *Duvall and Clark*, 2010; *Harkins et al*., 2010]. We used a Trimble®R3 GPS system which includes a base station antenna and receiver and two mobile, back-pack mounted units. For each set of surveys, the stationary base station received signals from satellites during the entire surveying process.

[13] We surveyed across three basaltic cinder cones that are cut by two major faults (Figure 3), in order to delineate the fault displacement geometry. We produced a number of closely spaced profiles across each fault by walking with the kinematic receivers perpendicular to the strike of the faults. The receivers automatically record the horizontal and vertical spatial coordinates every second. The profiles extend several tens of meters on either side of the fault in order to capture the geometry of the complicated surface of each cinder cone (CC). We measured 11 profiles on CC-1,

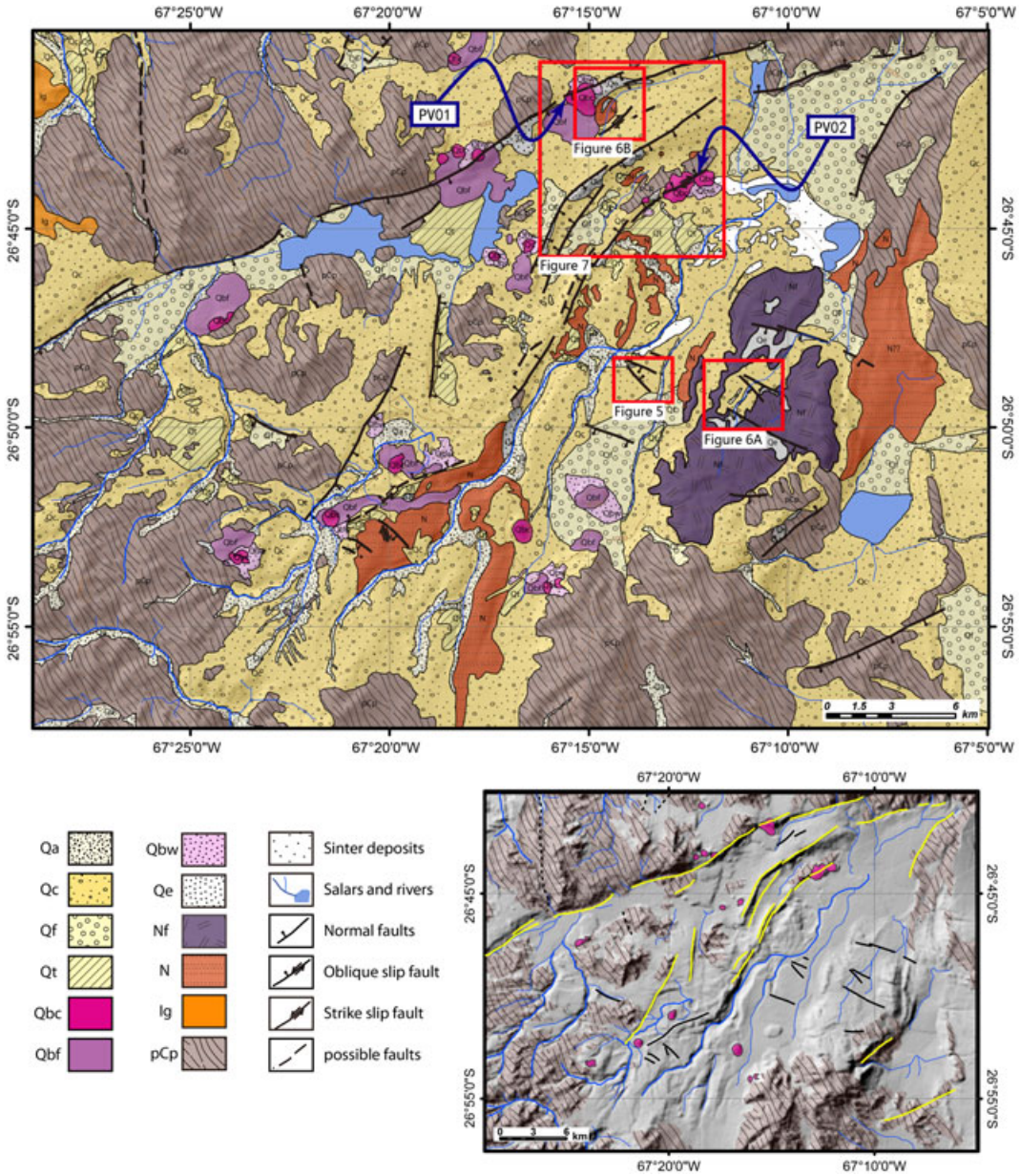

Figure 3. (top) Geomorphic and geological map of the Pasto Ventura region, NW Argentina. Location is shown in Figure 2.The base is a shaded relief map generated from 90 m STRM DEM data. (bottom) Simplified map showing two different fault groups distinguished in this study. Black lines represent Group 1, and the yellow lines represent Group 2. The metamorphic bedrock is shown in brown, patterned colors, while the cinder cones are shown in pink. Legend: Qa, Quaternary alluvial sediments; Qc, Quaternary colluvial sediments; Qf, Quaternary fluvial channel sediments; Qt, Quaternary terraces; Qbc, Quaternary basalt cinder cones; Qbf, Quaternary basalt flows; Qbw, Quaternary eolian volcanic clasts; Qe, Quaternary eolian sands; Nf, Neogene(?) lava flows; N, Neogene strata; Ig, Ignimbrite; pCp, pre-Cambrian bedrock.

10 on CC-2 and 5 on CC-3 with a horizontal spacing of approximately 50 m. Two additional profiles along a channel within CC-2 and along the eastern edge documented right-lateral displacement as well (Figure 4).

[14] To process the data, we first applied the error recorded by the stationary receiver to the profiles obtained during the surveying period. By this process, the floating points due to the factors such as satellite geometry and atmospheric interference are removed and the error level for the recorded spatial coordinates is lowered to less than a centimeter. In order to compensate for minor deviances in walking the profiles in the field, we fit straight lines to each of the profiles in map view, and then projected the elevation values to this best fit line (Figures S2 and S3). The surface of the cinder cones is highly irregular, thus a single profile is not likely to catch the true offset such as it could for a flat surface such as a river terrace. We analyze each profile individually and in the context of adjacent profiles

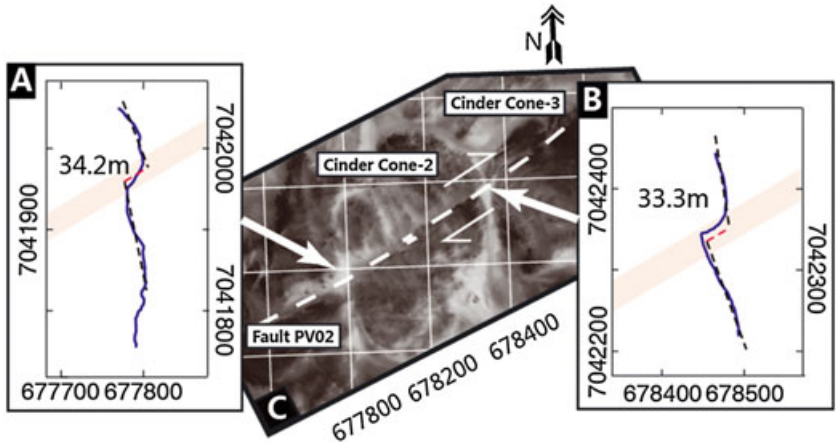

Figure 4. (c) Horizontal offset along Fault PV02 revealed by kinematic GPS surveying. Fault PV02 is marked by dashed white line. Measurements were taken at two offset features on Cinder Cone 2: (a) a displaced channel and (b) a displaced cinder cone edge. Blue lines in Figures 4a and b show the actual tracks of kinematic GPS receiver data, and the dashed black straight lines are best fits to the GPS tracks. Pink zones in Figures a and 4b define the fault zone. Horizontal offsets are determined along the strike of the fault (N60°E). Coordinates in Figures 4a–4c are all Universal Transverse Mercator (UTM) coordinate system, in Zone 19J, in meters.

and exclude those that cross anomalously high or low topography. The compilation of profiles allows us to conclude the reasonable ranges of the vertical offsets of those faults (Figures S4 and S5).

3.3. The $^{40}Ar/^{39}Ar$ Geochronology

[15] We dated the three samples collected from each of the Cinder Cones (CC) – 1, 2, and 3, using $^{40}Ar/^{39}Ar$ geochronology. The $^{40}Ar/^{39}Ar$ analyses were performed at the USGS in Denver, Colorado (detailed methods are given in the auxiliary material).[1] Sample P07-PV1-01 was collected from a lava flow that flows from the cinder cone (CC-1) that is cut through by Fault PV01 (Figures 3 and 7). Samples P07-PV2-01 and P07-PV2-02 were collected immediately adjacent Fault PV02 that cuts through CC-2 and CC-3, respectively (Figure 7).

4. Results

[16] In this paper, we document normal and strike-slip faults in the Pasto Ventura region which can be divided into two groups (Figure 3): (1) recently formed Quaternary normal faults and strike-slip faults and (2) pre-Quaternary reverse faults reactivated in the Quaternary as normal faults. These are discussed in turn, followed by an examination of regional fault kinematics and rate.

4.1. Fault Group 1: Recently Formed Quaternary Normal and Strike-Slip Faults

[17] We document a distinct group of normal faults that developed in Quaternary units (Figure 3). Perhaps because of their relatively small length and offset, these faults have not been previously recognized. The best example of these faults is in the central part of the map, which is covered by Quaternary colluvial sediments (Figure 3). The faults are marked by disrupted minor river channels that split into several channels where they flow across the fault from the footwall to the hanging wall (Figure 5), typical of fluvial channel interactions with active faults [*Burbank and Anderson*, 2001]. The horst-and-graben morphology and the lack of any apparent laterally offset channels lead us to infer dominantly dip-slip displacement. The channels are clearly inscribed in the surface and any horizontal offset would be immediately apparent, both in the field and in the remote imagery. The northern ends of both faults are eroded into by tributaries to a large canyon, allowing a rare opportunity to measure the orientation of minor faults, and demonstrating that the faults continue through the Quaternary cover into underlying Neogene strata (Figure 5). The minor faults display vertical offsets of only 20–30 cm and their dips are relatively steep (50°–70°) (Figure 5) (Table S1 in the auxiliary material). However, we did not find well-exposed fault surfaces or kinematic indicators. Similar faults occur in the southeast quadrant of the map as well, cutting Quaternary surfaces. In the eastern part of map area, several normal faults are identified in an andesitic lava flow, partially covered by colluvial sediments (Figure 6). The normal faults found in this area are of similar orientation, length and character to those developed entirely within Quaternary units. The footwalls of the normal faults have subsided, leading to the accumulation of dark colored, fine-grained sediments adjacent to the fault in the downthrown block. Additionally, we also found several Quaternary strike-slip faults in the Pasto Ventura region, marked by horizontally offset river channels: the faults strike approximately NW-SE and show right-lateral movement (Figure 6).

[18] Additional normal faults may be present within bedrock, but are difficult to identify because Group 1 faults are relatively short and have small displacement, which is easily obscured within the fractured, multiply deformed Ordovician Puncoviscana formation. On the other hand, the strength of the metamorphic rocks might lower the probability of developing small faults within bedrock. Further, the second group of faults, Group 2, which bound the metamorphic outcrops, likely accommodates the regional strain associated with bedrock outcrops.

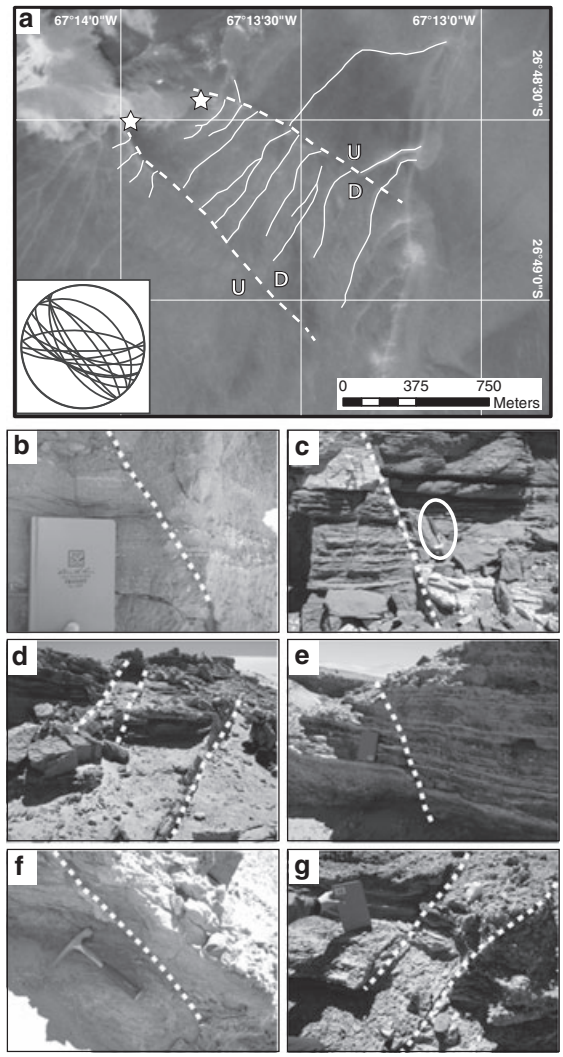

Figure 5. Group 1 normal faults in the central Pasto Ventura region. (a) Faults and adjacent river channels on air photo base. Inset shows fault plane measurements in the locations marked by stars (Table S1). The upthrown sides of the faults are marked by "U", while the down-thrown sides are marked by "D". Location is shown in Figure 3. (b–g) Field photos taken of minor faults at the location marked by stars.

4.2. Fault Group 2: Pre-Quaternary Reverse Faults Reactivated in the Quaternary

[19] In the Pasto Ventura region, there is a distinct second set of faults which appear to not be newly formed but rather to have reactivated older structures developed in the metamorphic bedrock [e.g., *Allmendinger et al*., 1989; Schoenbohm and Carrapa, 2011]. Some of these faults have been previously identified and described by *Allmendinger et al.* [1989] and *Marrett et al*. [1994]. They are longer than the faults in Group 1 and generally run within or along the edge of bedrock, rather than within Quaternary sediments. These faults strike roughly NNE-SSW, with some curvature (Figures 3 and 7). Although Group 2 faults are present throughout the map area, we focus on two prominent faults (Fault PV01 and Fault PV02) which also cut cinder cones (Figure 7). Fault PV01 linearly cuts through the north region of this map. The north block is mainly composed of metamorphic bedrock and the southern part is covered by fluvial and colluvial sediments, and as well as modern salars. Slightly to the south of Fault PV01, Fault PV02 curves from striking N20°E in the north to N55°E in the south. It also bounds metamorphic bedrock on the north side [*Allmendinger et al*., 1989]. Fault planes are poorly exposed, but relatively steep dips can be inferred from their linear traces. Previous studies of Fault PV02 indicate that it dips northwest and carried Puncoviscana basement over Neogene sediments in a reverse sense, but that it has been recently reactivated in a normal sense [*Allmendinger et al*., 1989; Schoenbohm and Carrapa, 2011]. Given the similarity in character, orientation and location, it is reasonable to conclude that all Group 2 faults are undergoing normal-oblique faulting and likely reactivate older reverse faults.

[20] Three young mafic cinder cones are offset by Fault PV01 and Fault PV02 during the extensional reactivation of the two faults, supported by the ages presented in this work. We measured topographic profiles (Figures S3, S4 and S5) across Faults PV01 and Fault PV02. We eliminated

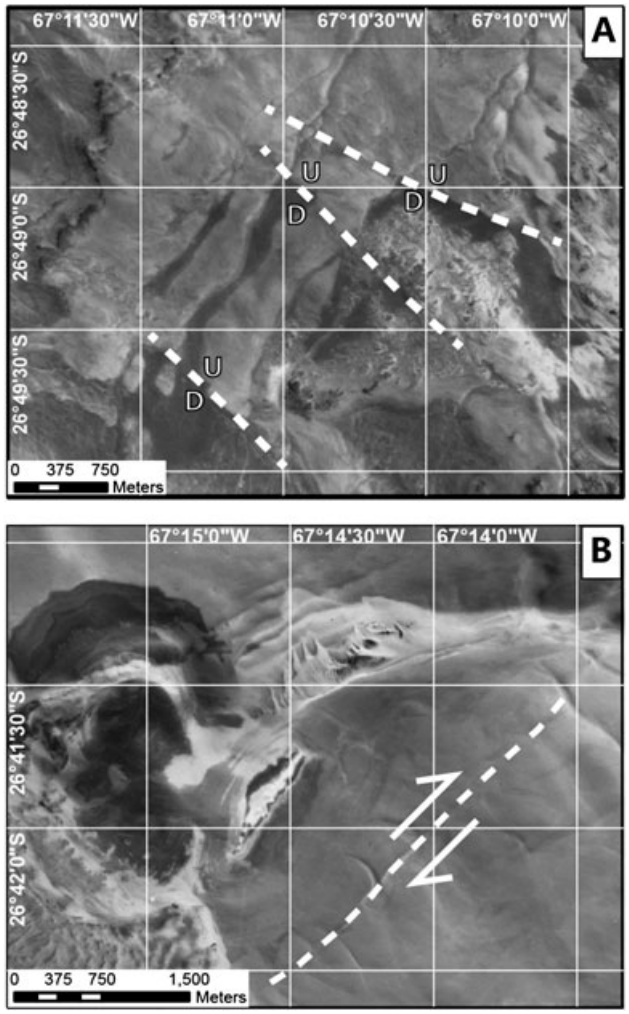

Figure 6. (a) Group 1 normal faults in the eastern Pasto Ventura region. The up-thrown sides of the faults are marked by "U", while the down-thrown sides are marked by "D". Location is shown in Figure 3. (b) Strike-slip fault developed during Quaternary near Cinder Cone 1 (CC-1). Arrows show direction of movement. The location is shown in Figure 3.

a number of profiles, which capture anomalous irregular topography of the cinder cone surface (Figure 8). For the remaining profiles, we determine the vertical displacement and uncertainty as follows (Figure 9 and Table S2). For most cases, we determined the elevation of the upthrown block by identifying the inflection point between the relatively horizontal surface of the cinder cone and the sloped faulted margin. The elevation of the downthrown block is complicated by erosion, which is concentrated in a zone close to the fault because of the localized weakness, resulting in the topographic low along the faults (Figure 9). The elevation of the downthrown block is thus determined by the location of the inflection point between the relatively horizontal surface on the downthrown block and the erosional slope above the fault, where present. The minimum is the bottom of the eroded trough along the fault and the maximum is the maximum topography present in the downthrown block. For profiles E-E', F-F' and G-G' across Fault PV02, observations from the DEM and field suggest they cut through the southern side of the cinder cone, which slopes south. As a result, on these profiles the footwall is higher than the hanging wall (Figure 9b). In this case, the inflection point is invisible on the profile, and we thus choose the lowest spot as the value for the downthrown block elevation. The preferred value for vertical offset is determined by subtracting the downthrown block elevation from the upthrown block elevation and using the maximum and minimum values of each to calculate the maximum and minimum possible offset.

[21] Finally, we compile the vertical offsets of the acceptable profiles to determine ranges of vertical offsets for the Fault PV01 and Fault PV02. We conclude here the vertical offset for the Fault PV01 is 9.8 +2.9/−3.1 m (Figure 8). Fault PV02 cuts through two cinder cones (CC-2 and CC-3). The profiles show the north side is the downthrown block, and the fault is inferred to dip north from the shape of the profiles (Figure 9). The 6 profiles on CC-2 shows that the vertical offset is 16.1 +2.7/−3.1 m, and the vertical offset based on two profiles for the CC-3 is 10.8 +5.0/−3.8 m. We also measured the horizontal offset component of CC-2 along Fault PV02. The horizontal traces for the offset

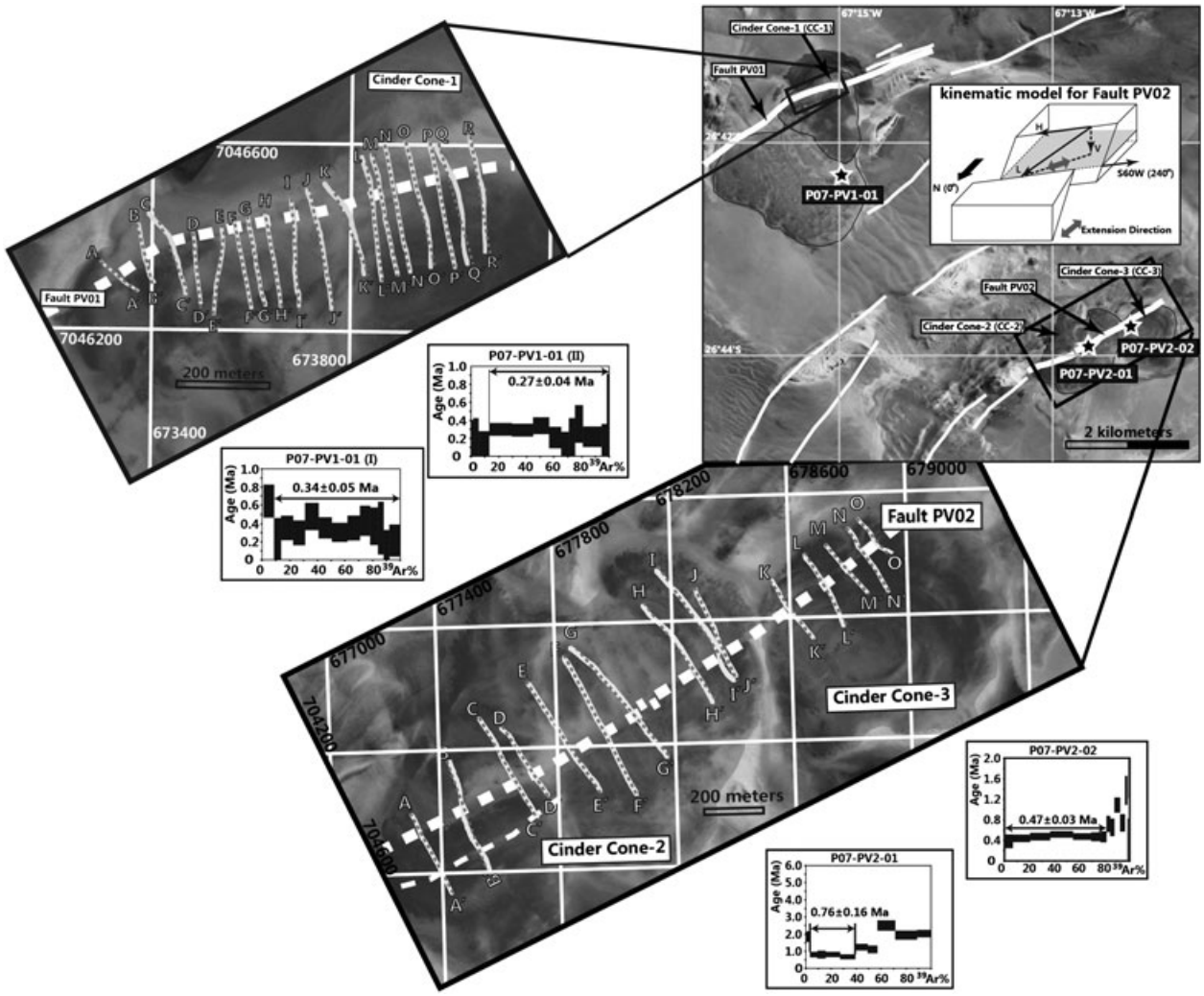

Figure 7. Detailed map (location shown in Figure 3) of Group 2 faults offsetting basaltic cinder cones and flows and kinematic GPS surveying across Fault PV01 and PV02. Faults are marked in white, with Faults PV-01 and PV02 highlighted. Stars mark sample locations. On the cinder cones, solid lines represent the actual measurement tracks taken in the field, while the dashed lines are fit straight lines. The $^{40}Ar/^{39}Ar$ results for basalt samples marked by stars are shown in insets. All features are shown on air photo base (InstitutoGeograficoMilitar, Argentina). Inset shows kinematic model for Fault PV02. Note that the current normal faulting took place along a pre-existing fault plane. Extension direction can be determined by geometric calculations.

cinder cone edge and the channel on it show this fault have been moved 34±1 m right laterally (Figure 4).

4.3. Kinematics of Recent Extension in the Pasto Ventura Region

[22] Ideally, to determine the kinematics of recent deformation, we would locate fault plane exposures and measure the orientation and slip features directly. However, the study area is covered by Quaternary colluviums and eolian sediments, river exposures are limited in depth, and wind erosion of surface features is significant. Therefore exposures of fault planes suitable for kinematic measurements are virtually nonexistent. Moreover, one or few measurements from secondary faults or reactivated fault planes could be insufficient or even misleading, given the multiple phases of deformation in this region [*Allmendinger et al*., 1997, and references therein; *Marquillas et al*., 2005]. Though the direct fault-plane-derived slip information is difficult to find, kinematics of recent extension in this region is vital and thus has to be constrained to some degree. In this study, we focus on solving the extension direction in the horizontal plane (we refer to this as "horizontal extension"), using two independent approaches in the Pasto Ventura region. The consistent results from these two methods lead us to propose that the Pasto Ventura region is currently undergoing NE-SW to NNE-SSW horizontal extension.

[23] First, because they are young, short and mostly linear and they are not influenced by previous generations of deformation, the orientation of the 13 normal faults in Group 1 provides direct clues for the horizontal extension direction. We make the simplifying assumption that the normal faults accommodated pure dip-slip displacement. The few instances of kinematic data collected from these faults confirm this assumption. If there is no strike-slip displacement, then the

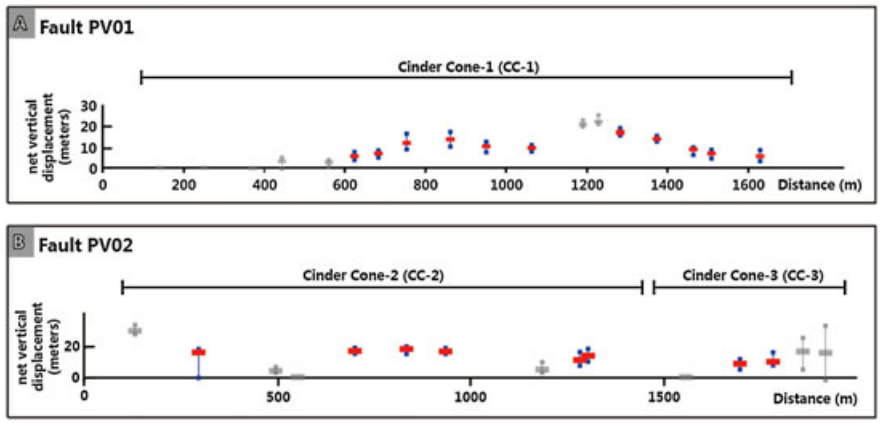

Figure 8. Vertical fault displacement of Fault PV01 and Fault PV02 revealed by kinematic GPS surveying. Gray data points are excluded from averages because of anomalously high topography in the hanging wall or footwall or erosion.

net slip vector must be the same as the dip slip vector. We compile the orientation of the net slip vector for the 13 normal faults in a rose diagram (Figure 2 inset and Table 1). The directions are clustered about a NNE-SSW orientation (Figure 2 inset). This result is supported as well by our observation and measurement on the minor faults associated with two normal faults in the central part of the map (Figure 6).

[24] Second, we perform a geometric calculation on the normal and strike-slip component of displacement obtained from CC-2 along Fault PV02. Group 2 faults originally formed by thrust faulting before the late Miocene [*Allmendinger et al*., 1989; *Marrett et al*., 1994; *Allmendinger et al*., 1997], thus orientation alone may not directly reflect the stress field under which they are currently active. The cinder cones we surveyed are < 0.8 Ma in age, thus the displacement reflects only recent horizontal extension. We assume the fault plane for PV02 dips NW-NNW based on the surface geometry measured in this study and other investigations of the same fault [*Schoenbohm* and *Carrapa*, 2011]. Because we do not have empirical evidence for the fault dip at this location, we apply a range of values, taking 45° as the lower limit because any lower dip would lead to a curved rather than linear trace across the topography, and 70° as an upper limit based on the dip observed by *Schoenbohm* and *Carrapa*, 2011. The calculation based on the geometric relationship between vertical offset, horizontal offset, and fault plane strike and dip (Figure 7) indicates that the overall horizontal net slip vector across Fault PV02 ranges from N30°E to N52°E, depending on the dip of the fault (Figure 2 inset). This result is consistent with the compilation of Group 1 normal faults (Figure 2 inset).

[25] The consistency of the results from analyzing Groups 1 and 2 faults lead us to propose the horizontal extension direction in the Pasto Ventura region is NE-SW to NNE-SSW. Although some previous studies in the Pasto Ventura region agree with our results [e.g., *Montero Lopez et al*., 2010], others disagree. *Allmendinger et al*. [1989] and *Marrett et al*. [1994] document NNW-SSE extension in the Pasto Ventura region based on lineation measurements on exposures of the fault plane along Fault PV01. However, as Fault PV01 was reactivated, and fault kinematic indicators such as lineations on the fault planes may not represent the current stage of extension, these studies may not capture the true recent fault kinematics [*Allmendinger et al*., 1989; *Cladouhos et al*., 1994; *Marrett et al*., 1994; *Allmendinger et al*., 1997].

[26] Note that we do not calculate the shortening direction for the faults in the Pasto Ventura region. Although the presence of strike-slip and normal faults suggests that the region could be undergoing subhorizontal contraction, consistent with some plateau-wide deformation models [e.g., *Riller and Oncken*, 2003], the absence of thrust or reverse faulting in the Pasto Ventura region argues in favour of vertical shortening. The issue remains unresolved.

4.4. Timing and Rate of Extension

[27] Faults PV01 and Fault PV02 offset three basaltic cinder cones, so by determining the eruption ages of the cinder cones we place maximum ages on these displacements. Here we report CO_2 laser incremental heating $^{40}Ar/^{39}Ar$ ages for these three cinder cones (Figure 7). Our best estimates for the eruption ages for these cinder cones come from the $^{40}Ar/^{39}Ar$ plateau ages determined for each sample, which are ideally calculated from two or more contiguous heating steps with statistically indistinguishable ages and together represent >50% of the ^{39}Ar released. Sample P07-PV1-01 from Cinder Cone 1 was run twice following the same procedure and produced $^{40}Ar/^{39}Ar$ plateau ages of 0.34 ± 0.05 and 0.27 ± 0.04 Ma (2σ), which are within error (Figure 6). The sample was run twice to check internal sample precision, because low radiogenic ^{40}Ar contents are known to contribute to imprecision in $^{40}Ar/^{39}Ar$ ages of young basaltic volcanic rocks [e.g., *Duncan and Hogan*, 1994; *Spell and McDougall*, 2003; *Singer et al*., 2004; *Wang et al*., 2006]. Cinder Cone 3 (CC-3) has a well-defined $^{40}Ar/^{39}Ar$ age plateau of 0.47 ± 0.03 Ma (2σ) (Figure 7). No strict $^{40}Ar/^{39}Ar$ plateau age was determined for Cinder Cone 2 (CC-2) following the criteria mentioned above; however, a forced $^{40}Ar/^{39}Ar$ plateau age of 0.76 ± 0.16 Ma (Figure 7) was calculated for four heating steps that included ~40% of the total ^{39}Ar released.

[28] Fault PV02 offsets CC-2 (circa 0.8 Ma) by 16.1 +2.7/−3.1 m and CC-3 (circa 0.5 Ma) by 10.8 +5.0/−3.8 m (Figure 8) by extensional faulting. Since the cones are displaced different amounts, faulting must have been active between 0.5 and 0.8 Ma, and must have continued afterward as well. As constrained by the age of the displaced CC-1,

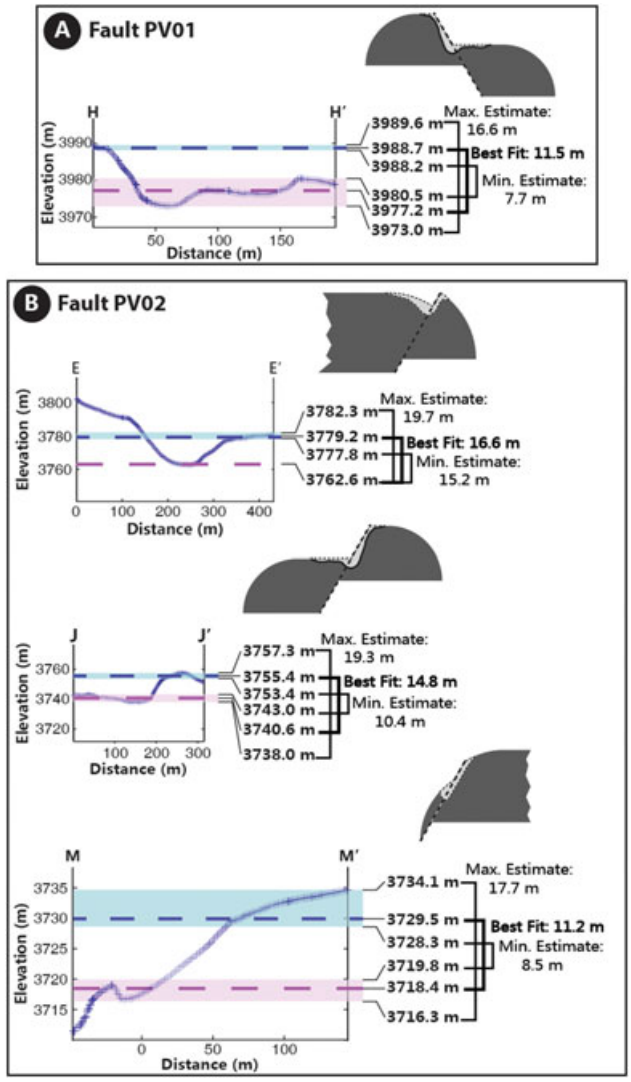

Figure 9. Representative profiles from GPS survey and interpreted model. Profile locations indicated in Figure 6. Hanging wall–footwall geometry depends on fault orientation and where the fault intersects the curved surface of the cinder cone. Maximum, minimum and best fit elevations determined as described in text. All profiles can be found in Figures S4 and S5.

Fault PV01 has been active at least since circa 0.3 Ma. Likely, both faults were active before 0.8 Ma, as other studies indicate the whole region has undergone horizontal extension since the late Miocene to Pliocene [*Kay et al*., 1994; *Allmendinger et al*., 1997; *Riller et al*., 2001; *Schoenbohm and Strecker*, 2009, and references therein].

[29] Our calculation based on inferences about the fault geometry and displacement measured using the GPS profiles constrains the horizontal component of displacement vector in this area to 33.4–38.9 m across Fault PV02, along N26°E to N56°E (Figure 7). This yields an average horizontal extension rate of 0.04–0.08 mm/yr since 0.8 Ma. For CC-3, also cut by Fault PV02, we calculate its extension rate based on the known vertical offset and the same direction determined by CC-2 data, yielding an extension rate of 0.02–0.04 mm/yr, slightly lower than but consistent with the results from CC-2. Because Fault PV02 offsets two different-aged cinder cones by different amounts, influence from episodic fault movements is minimized in our analysis. Further, although we cannot constrain the horizontal displacement of CC-1 by Fault PV01, and therefore cannot calculate horizontal extension rate, the amount of vertical displacement across CC-1 is comparable to the similarly aged CC-3, offset by Fault PV02. We therefore infer a similar slip rate on Fault PV01, assuming both faults have a similar dip and are extending in the same stress regime. Although the uncertainties on our calculations are relatively large because of the lack of exposure of the fault plane and the irregularity of the offset surfaces, we demonstrate NNE-SSW to NE-SW extension at a slow rate of 0.02–0.08 mm/yr since at least circa 0.5 Ma.

5. Discussion

[30] The extension across the Altiplano-Puna Plateau is widespread [*Allmendinger*, 1986; *Allmendinger et al*., 1989; *Marrett and Emerman*, 1992; *Mercier et al*., 1992; *Cladouhos et al*., 1994; *Kay et al*., 1994; *Marrett et al*., 1994; *Allmendinger et al*., 1997; *Riller and Oncken*, 2003; *Baldwin*, 2005;

Table 1. Group 1 Fault: Recently Formed Quaternary Normal and Strike-Slip Faults[a]

No.	Normal or Strike Slip	Length (km)	Strike (deg)	Location
1	normal fault	2.5	290.75	S26.8359; W67.2413
2	normal fault	1.6	315.86	S26.8124; W67.2298
3	normal fault	1.3	293.38	S26.8089; W67.2251
4	normal fault	0.5	288.44	S26.8025; W67.2229
5	normal fault	6	291.68	S26.7922; W67.1681
6	normal fault	1.5	297.03	S26.8187; W67.1710
7	normal fault	1.6	318.37	S26.8188; W67.1807
8	normal fault	4.3	296.37	S26.8410; W67.1665
9	normal fault	1.9	271.02	S26.8626; W67.1853
10	normal fault	2	312.42	S26.8815; W67.3290
11	normal fault	0.7	341.57	S26.8813; W67.3334
12	normal fault	1.3	305.36	S26.8908; W67.3499
13	normal fault	2.5	297.58	S26.8355; W67.3796
14	strike-slip fault	2.9	62.26	S26.8642; W67.3343
15	strike-slip fault	6.3	61.61	S26.7056; W67.2377

[a]The faults are shown on Figure 3 (numbers are given in auxiliary material). The length and strike of each fault is determined on image data.

Schoenbohm and Strecker, 2009; *Montero Lopez, et al*., 2010; *Santimano and Riller*, 2012]. Our study is the first to constrain the extension rate on any normal fault on the Puna Plateau. We find an extremely slow, time-integrated rate of extension. If this rate is characteristic of other normal and strike-slip faults on the Puna Plateau, the accumulated horizontal extension is limited in magnitude. As discussed by *Marrett and Allmendinger* [1992], small faults could contribute significantly to our estimation for regional deformation because they are large in number. However, if the rate we find of a single fault in the Pasto Ventura region is characteristic of faults across the plateau, given the density of faulting, the overall rate of plateau-wide horizontal extension would still be much lower than observed in other plateau regions around the world. For example, rates in the Puna appear to be lower in the other major plateau on Earth. In central Tibet, E-W extension is accommodated by NE striking left-slip faults to the north and NW striking right-slip faults to the south of the Bangong-Nujiang suture zone [*Taylor et al*., 2003; *Taylor and Peltzer*, 2006]. Field and image studies suggest a 5–6 mm/yr slip rate for the conjugate strike-slip faults [*Taylor and Peltzer*, 2006], constraining horizontal displacement rates to the order of 1 mm/yr. In the Shuanghu Suture zone, central Tibet, investigation and modeling of a normal fault scarp reveal that the minimum slip rate on this fault is 2 mm/yr since 2 ka [*Avouac and Peltzer*, 1993; *Yin et al*., 1999]. Another study on the Shuanghu Graben system indicates that during late Quaternary the total rate of vertical displacement could be no more than 0.3 mm/yr [*Blisniuk and Sharp*, 2003], which leads to the extension rates constrained at about 0.2–0.3 mm/yr. In the southern Tibetan Plateau, the Yadong-Gulu graben system underwent a cumulative vertical displacement of graben-bounding normal faults during the Quaternary at a rate of 1.9±0.6 mm/yr [*Armijo et al*., 1986; *Armijo et al*., 1989].

[31] There have been several major GPS projects in South America, including CASA [e.g., *Kellogg and Dixon*, 1990], SNAPP [e.g., *Leffler et al*., 1997; *Norabuena et al*., 1998], SAGA [e.g., *Khazaradze and Klotz*, 2003], CAP [e.g., *Kendrick et al*., 2001] and ANSA [e.g., *Klotz and Lelgemann*, 1988]. These clearly document shortening within the modern cordillera mountain front [e.g., *Leffler et al*., 1997; *Norabuena et al*., 1998; *Kendrick et al*. 2001]. However, despite these extensive networks, there are only three GPS monuments on the southern Puna Plateau (From SAGA, Figure 2) [*Khazaradze and Klotz*, 2003]. Almost all of the stations and reported data are from the western and eastern Cordilleras or to the north. The existing stations within the southern Puna have not recorded any relative motion between each other, when we take the measurement error into consideration [*Leffler et al*., 1997; *Norabuena et al*., 1998; *Brooks et al*., 2003; *Kendrick et al*., 2001; *Bevis et al*., 2001]. This implies that the plateau is either stable, or it is undergoing only very subtle deformation. The abundance of active faults on the plateau suggests that some deformation is occurring; the slow rates we document in this study are consistent with the lack of obvious deformation in the GPS data.

[32] Our study documents a NE-SW to NNE-SSW directed horizontal extension of the Pasto Ventura region. Our result in the Pasto Ventura region is in general agreement with other regional studies of the Puna Plateau (Figure 2). *Schoenbohm and Strecker* [2009] document fault plane measurements on the Punta Negra fault to the east, and show that the NW segment of the Punta Negra fault has been reactivated more recently as a normal fault. The limited kinematic data suggests oblique or strike-slip displacement and likely NE-SW to ENE-SWS extension [*Schoenbohm and Strecker*, 2009]. *Baldwin* [2005] also document NE-SW extension during Pliocene and Quaternary time on the southern margin of the Puna Plateau in the Buena Ventura region. However, the horizontal extension direction is not consistent to the north. In the Antofalla Basin and areas further north on the Puna Plateau, *Marrett et al*. [1994] propose NNW-SSE extension following a WNW-ESE shortening phase; they argue this subhorizontal extension is evident as far as the northern part of the Puna and the southernmost Altiplano. Observations that are off but close to the plateau area display similar results. In the Bolsón de Fiambalá region and Pipanaco region to the south, horizontal extension directions are inferred to be NE-SW to NNE-SSW from normally reactively structures [*de Urreiztieta et al*., 1996; *Montero Lopez et al*., 2010]. In the Eastern Cordillera, Quebrada del Toro–Solá Fault shows NW-SE extension since 4.17 Ma [*Marrett and Strecker*, 2000]. *Santimano and Riller* [2012] document that both the Cachi and Calchaqui faults have a experienced NE-SW extension during Quaternary. These locations are not on the plateau, as defined by the smoothed 3000 m topographic contour or the boundary of internal drainage, however, and therefore may be subject to different geodynamic forcings. We therefore deemphasize these data in our subsequent analysis. Overall, currently documented extension directions for the southern Puna Plateau display great variability, with directions differing from each other by up to 90°.

[33] A number of different models have been proposed to explain the extension observed in the Puna Plateau. An important proposal is that widespread normal faulting could be a precursor to more extensive gravitational spreading [*Schoenbohm and Strecker*, 2009] in the Central Andean Plateau, such as is now widespread in the Tibetan Plateau [*England and Houseman*, 1989; *Blisniuk et al*., 2001; *Rey et al*., 2001; *Royden et al*., 2008]. If this were the case, a relationship between the extension direction and the average plateau orientation is expected (either E-W extension, or extension perpendicular to the margin of the plateau) [*Schoenbohm and Strecker*, 2009]. However, as documented

by this study, two trends of extension are observed in the Puna Plateau, implying more complex, localized causes for horizontal extension.

[34] A second possibility is a large component of plan view simple shear of the plateau [*Riller and Oncken*, 2003; *Riller et al*., 2012] which could result from a decrease in crustal shortening of >200 km from the center of the Central Andean Plateau to a few tens of kilometers in the southern Puna [*Kley and Monaldi*, 1998]. The strain ellipse for such deformation would suggest a maximum principle strain (contraction) oriented WNW-ESE and a minimum principle strain (extension) oriented NNE-SSW, accommodated on NW to north trending, orogen-parallel, sinisterly reactivated faults and NE trending, newly formed, dextral faults [*Riller and Oncken*, 2003; *Riller et al*., 2012]. Both transpression and transtension are possible in this model, depending on the specific fault orientation. Our data from the Pasto Ventura region are consistent with this model, although we don't observe the same rhomb-like geometry created by the intersection of the two fault trends identified by *Riller and Oncken* [2003]. However, some horizontal extension to the north of 26°S is inconsistent with this model, as it is dominantly oriented NW-SE [*Marrett et al*., 1994; *Marrett and Strecker*, 2000]. This may be due to the local strain heterogeneity such that the local extension may only reflect local kinematics of deformation directions [e.g., *Santimano and Riller*, 2012] or could be due to more complex regional geodynamic background.

[35] A third, widely cited model for subhorizontal extension of the Puna Plateau is lithospheric foundering [e.g., *Kay et al*., 1994; *Babeyko and Sobolev*, 2005; *Oncken et al*., 2006; *Schurr et al*., 2006]. The scenario that part of the lower lithosphere beneath the Puna Plateau has foundered has been supported by various studies including geophysical [*Whitman et al*., 1992, 1996; *Yuan et al*., 2002; *McGlashan et al*., 2008] and geochemical [*de Silva*, 1989; *Kay et al*., 1999; *Kay and Coira*, 2009; *Kay et al*., 2009; *Kay et al*., 2010] ones. However, the mechanisms of the lower lithospheric foundering of the Puna Plateau have not been discussed. The foundering processes could take place via either delamination or "dripping" of the lower lithosphere [*Bird*, 1979; *Houseman et al*., 1981; *Göğüş and Pysklywec*, 2008]. In delamination, the delaminating slab migrates perpendicular to the line of initiation, causing surficial deformation to migrate across the affected area with a consistent orientation [*Bird*, 1979; *Bird and Baumgardner*, 1981; *Pysklywec and Cruden*, 2004; *Göğüş and Pysklywec*, 2008; *Pysklywec et al*., 2010]. In contrast, during the formation of a Rayleigh-Taylor type instability [*Houseman et al*., 1981], uplift and subsidence of the plateau surface, and contraction and extension of the upper crust are all symmetric about the lower lithospheric "drip," and thus would vary significantly in orientation (see schematic illustration in the auxiliary material) [*Göğüş and Pysklywec*, 2008]. Our compilation of horizontal extension directions shows that the horizontal extension on the Puna is not subparallel but rather exhibits trends north and south of approximately 26°S (Figure 2). Thus, if recent extension in the Puna reflects lithospheric foundering, it is likely the result of dripping rather than delamination. Furthermore, the ages of basaltic volcanism throughout the Puna Plateau show that the oldest eruptions (as old as 7.3 Ma) are clustered in the central of southern Puna Plateau, also near 26°S, becoming younger both north and south of this line (Figure 2) (*Kay et al*. [1994]; *Risse et al*. [2008], and data herein). This pattern can be explained by the formation of a Rayleigh-Taylor type instability centered at 26°S beneath the Puna Plateau since the mid-Miocene (Schoenbohm and Carrapa, 2011).

[36] Finally, special circumstances related to the position of the Pasto Ventura region within the Puna Plateau could explain recent horizontal extension. The Culampaja transverse zone trends approximately through our study region – these lineaments have been associated with volcanism and left-lateral transtensive fault zones elsewhere [e.g., *Riller et al*., 2001; *Petrinovic et al*., 2005]. Additionally, because of the position of the Pasto Ventura region on the very southern edge of the plateau, the high topographic gradient could enhance the effect of the gravitational spreading (the so-called "edge effect" [*Allmendinger et al*., 1997]). However, given the widespread nature of horizontal extension on the Puna Plateau, we consider multiple models to explain extension in the Pasto Ventura region.

[37] Given the wide range of processes which must be acting on the Puna Plateau, we suspect there is more than one cause for the recent formation of normal and strike-slip faults in the Pasto Ventura region, and across the Puna Plateau more generally. Because a strong case can be made for lithospheric foundering on the basis of geochemical and geophysical data [e.g., *Kay et al*., 1994; *Yuan et al*., 2002; *Tassara et al*., 2006; *McGlashan et al*., 2008; *Drew et al*., 2009], we suspect that this geodynamic factor plays a role in our study region. This is consistent with our observation of a systematic variation in horizontal extension directions north and south of 26°S, the location of an inferred late Miocene drip (Schoenbohm and Carrapa, 2011). However, given that horizontal extension is found throughout the entire Central Andean Plateau, gravitation spreading of the elevated upper crust is also a viable possibility [*Schoenbohm and Strecker*, 2009], and could contribute in our study region as well. Finally, NNE-SSW to NE-SW extension in the Pasto Venture region is consistent with plan view simple shear of the plateau [e.g., *Riller and Oncken*, 2003], although this model cannot be the only explanation for normal faulting in the Puna because of the apparently different horizontal extension directions observed north of 26°S within the confines of the modern plateau.

6. Conclusion

[38] In this study, we examine two groups of faults in the Pasto Ventura region, NW Argentina. The analysis of the small, newly developed faults and high-angle reverse faults recently reactivated as normal faults shows that the Pasto Ventura region has been extending subhorizontally toward the NE-SW to NNE-SSW since at least ~0.5 Ma. We document a low extension rate of 0.02–0.08 mm/yr across a single fault. This is the first quantitative study of extension rate on the Puna Plateau and to our knowledge is the lowest documented extension rate on a normal fault in any plateau region around the globe.

[39] Our data can fit several important models for the origin of extension on the Puna Plateau, including gravitational spreading of the elevated lithosphere, edge effects due to the topographic gradient between the southern Puna Plateau and the adjacent lowlands, plan view simple shear of the plateau

and lower lithospheric foundering. Although data from the Pasto Ventura region alone are consistent with most of these models, lithospheric foundering through a drip centered at 26°S, best explains the observed regional deformation pattern. Given the complex geological and geodynamic factors operating within the Puna Plateau, more work needs to be done in order to evaluate the relative importance of these models.

[40] **Acknowledgements.** This work is funded by an NSERC-Discovery grant to L.S. We thank F. Zambrano and S. Cavolo for assistance in the field and J. Dortch, R. Pysklywec and P.-Y. Robin for useful discussions. The constructive and critical reviews from U. Riller and an anonymous reviewer have fundamentally improved this manuscript.

References

Acocella, V., A. Gioncada, R. Omarini, U. Riller, R. Mazzuoli, and L. Vezzoli (2011), Tectono-magmatic characteristics of the Calama-Olacapato-El Toro Fault Zone (Puna and Eastern Cordillera), Central Andes, *Tectonics*, *30*, TC3005, doi:10.1029/2010TC002854.

Allmendinger, R. W. (1986), Tectonic development, southeastern border of the Puna Plateau, northwestern Argentine Andes, *Geol. Soc. Am. Bull.*, *97*(9), 1070-1082.

Allmendinger, R. W., M. Strecker, J. E. Eremchuk, and P. Francis (1989), Neotectonic deformation of the southern Puna Plateau, northwestern Argentina, *J. South Am. Earth Sci.*, *2*, 111–130, doi:10.1016/0895-9811(89)90040-0.

Allmendinger, R. W., T. E. Jordan, S. M. Kay, and B. L. Isacks (1997), The evolution of the Altiplano-Puna Plateau of the central Andes, *Annu. Rev. Earth Planet. Sci.*, *25*, 139–174.

Armijo, R., P. Tapponnier, J. L. Mercier, and T. L. Han (1986), Quaternary extension in southern Tibet: Field observations and tectonic implications, *J. Geophys. Res.*, *91*(B14), 13,803–13,872.

Armijo, R., P. Tapponnier, and H. Tonglin (1989), Late Cenozoic right-lateral strike-slip faulting in southern Tibet, *J. Geophys. Res.*, *94*(B3), 2787–2838.

Arriagada, C., P. R. Cobbold, and P. Roperch (2006), Salar de Atacama basin: A record of compressional tectonics in the central Andes since the mid-Cretaceous, *Tectonics*, *25*, TC1008, doi:10.1029/2004TC001770.

Avouac, J.-P., and G. Peltzer (1993), Active tectonics in southern Xinjiang, China: Analysis of terrace riser and normal fault scarp degradation along the Hotan-Qira Fault System, *J. Geophys. Res.*, *98*(B12), 21,773–21,807, doi:10.1029/93JB02172.

Babeyko, A. Y., and S. V. Sobolev (2005), Quantifying different modes of the late Cenozoic shortening in the central Andes, *Geology*, *33*(8), 621–624, doi:10.1130/g21126.1.

Baldwin, A. K. (2005), Pliocene-Quaternary deformation and magmatism at the southern margin of the Puna Plateau, Argentine Andes, thesis, 234 pp., Univ. of Tex. at Austin, Austin.

Bevis, M., E. Kendrick, R. Smalley Jr., B. Brooks, R. Allmendinger, and B. Isacks (2001), On the strength of interplate coupling and the rate of back arc convergence in the central Andes: An analysis of the interseismic velocity field, *Geochem. Geophys. Geosyst.*, *2*(11), 1067, doi:10.1029/2001GC000198.

Bird, P. (1979), Continental delamination and the Colorado Plateau, *J. Geophys. Res.*, *84*(B13), 7561–7571.

Bird, P., and J. Baumgardner (1981), Steady propagation of delamination events, *J. Geophys. Res.*, *86*(B6), 4891–4903.

Blisniuk, P. M., and W. D. Sharp (2003), Rates of late Quaternary normal faulting in central Tibet from U-series dating of pedogenic carbonate in displaced fluvial gravel deposits, *Earth Planet. Sci. Lett.*, *215*(1–2), 169–186, doi:10.1016/S0012-821x(03)00374-1.

Blisniuk, P. M., B. R. Hacker, J. Glodny, L. Ratschbacher, S. W. Bi, Z. H. Wu, M. O. McWilliams, and A. Calvert (2001), Normal faulting in central Tibet since at least 13.5 *Myr ago, Nature*, *412*(6847), 628–632.

Borsa, A. A., H. A. Fricker, B. G. Bills, J. B. Minster, C. C. Carabajal, and K. J. Quinn (2008), Topography of the salar de Uyuni, Bolivia from kinematic GPS, *Geophys. J. Int.*, *172*(1), 31–40, doi:10.1111/j.1365-246X.2007.03604.x.

Brooks, B. A., M. Bevis, R. Smalley Jr., E. Kendrick, R. Manceda, E. Lauría, R. Maturana, and M. Araujo (2003), Crustal motion in the Southern Andes (26°–36°S): Do the Andes behave like a microplate?, *Geochem. Geophys. Geosyst.*, *4*(10), 1085, doi:10.1029/2003GC000505.

Burbank, D., and R. Anderson (2001), Tectonic Geomorphology, Blackwell Sci., Malden, Mass.

Burchfiel, B. C., and L. H. Royden (1985), North-south extension within the convergent Himalayan region, *Geology*, *13*(10), 679–682.

Cannon, M. E. (1990), High-accuracy GPS semikinematic positioning: Modeling and results, navigation, *Navigation*, *37*(1), 53–64.

Carrapa, B. and P. G. DeCelles (2008), Eocene exhumation and basin development in the Puna of northwestern Argentina, *Tectonics*, *27*, TC1015, doi:10.1029/2007TC002127.

Cladouhos, T. T., R. W. Allmendinger, B. Coira, and E. Farrar (1994), Late Cenozoic deformation in the central Andes—Fault kinematics from the northern Puna, northwestern Argentina and southwestern Bolivia, *J. South Am. Earth Sci.*, *7*(2), 209–228.

Coira, B., and S. M. Kay (1993), Implications of Quaternary volcanism at Cerro Tuzgle for crustal and mantle evolution of the Puna Plateau, central Andes, Argentina, *Contrib. Mineral. Petrol.*, *113*(1), 40–58.

Coira, B., J. Davidson, C. Mpodozis, and V. Ramos (1982), Tectonic and magmatic evolution of the Andes of northern Argentina and Chile, *Earth Sci. Rev.*, *18*(3–4), 303–332.

de Silva, S. L. (1989), Altiplano-Puna Volcanic Complex of the Central Andes, *Geology*, *17*(12), 1102–1106.

de Urreiztieta, M., D. Gapais, C. Le Corre, P. R. Cobbold, and E. Rossello (1996), Cenozoic dextral transpression and basin development at the southern edge of the Puna Plateau, northwestern Argentina, *Tectonophysics*, *254*, 17–39, doi:10.1016/0040-1951(95)00071-2.

Drew, S. T., M. N. Ducea, and L. M. Schoenbohm (2009), Mafic volcanism on the Puna Plateau, NW Argentina: Implications for lithospheric composition and evolution with an emphasis on lithospheric foundering, *Lithosphere*, *1*(5), 305-318, doi:10.1130/L54.1.

Duncan, R. A., and L. G. Hogan (1994), Radiometric dating of young MORB using the ^{40}Ar-^{39}Ar incremental heating method, *Geophys. Res. Lett.*, *21*(18), 1927–1930.

Duvall, A. R., and M. K. Clark (2010), Dissipation of fast strike-slip faulting within and beyond northeastern Tibet, *Geology*, *38*(3), 223–226, doi:10.1130/G30711.1.

England, P., and G. Houseman (1989), Extension during continental convergence, with application to the Tibetan Plateau, *J. Geophys. Res.*, *94*(B12), 17,561–17,579.

Göğüş, O. H., and R. N. Pysklywec (2008), Near-surface diagnostics of dripping or delaminating lithosphere, *J. Geophys. Res.*, *113*, B11404, doi:10.1029/2007JB005123.

Houseman, G. A., D. P. Mckenzie, and P. Molnar (1981), Convective instability of a thickened boundary-layer and its relevance for the thermal evolution of continental convergent belts, *J. Geophys. Res.*, *86*(86), 6115–6132

Harkins, N., E. Kirby, X. Shi, E. Wang, D. Burbank, and F. Chun (2010), Millennial slip rates along the eastern Kunlun fault: Implications for the dynamics of intracontinental deformation in Asia, *Lithosphere*, *2*(4), 247–266, doi:10.1130/L85.1.

Hilley, G. E., and M. R. Strecker (2005), Processes of oscillatory basin filling and excavation in a tectonically active orogen: Quebrada del Toro Basin, NW Argentina, *Geol. Soc. Am, Bull*,, *117*(7–8), 887–901, doi:10.1130/1325602.1.

Humphreys, E. (2009), Relation of fl at subduction to magmatism and deformation in the western United States, in Backbone of the Americas: Shallow Subduction, Plateau Uplift, and Ridge and Terrane Collision, edited by S. M. Kay, V. A. Ramos, and W. R. Dickinson, Mem. Geol. Soc. Am., 204, 85–98, doi:10.1130/2009.1204(04).

Kapp, P., and J. H. Guynn (2004), Indian punch rifts Tibet, *Geology*, *32*(11), 993–996, doi:10.1130/G20689.1.

Kay, R. W., and S. M. Kay (1993), Delamination and delamination magmatism, *Tectonophysics*, *219*(1–3), 177–189.

Kay, S. M., and B. L. Coira (2009), Shallowing and steepening subduction zones, continental lithospheric loss, magmatism, and crustal flow under the central Andean Altiplano-Puna Plateau, in Backbone of the Americas: Shallow Subduction, Plateau Uplift and Ridge and Terrane Collision, edited by S. M. Kay, V. A. Ramos, and W. R. Dickinson, Mem. Geol. Soc. Am., 204, 229–259, doi:10.1130/2009.1204(11).

Kay, S. M., B. Coira, and J. Viramonte (1994), Young mafic back arc volcanic-rocks as indicators of continental lithospheric delamination beneath the Argentine Puna Plateau, central Andes, *J. Geophys. Res.*, *99*(B12), 24,323–24,339.

Kay, S. M., C. Mpodozis, and B. Coira (1999), Magmatism, tectonism, and mineral deposits of the central Andes (22°–33°S latitude), in Geology and Ore Deposits of the Central Andes, edited by B. J. Skinner, Spec. Publ. SEPM Soc. Sediment. Geol., *7*, 27–59.

Kay, S. M., B. L. Coira, and R. W. Kay (2009), Central Andean Galan Ignimbrites: Magma evolution from the mantle to eruption in a thickened crust, *Geochim. Cosmochim. Acta*, *73*(13), A630.

Kay, S. M., B. L. Coira, P. J. Caffe, and C.-H. Chen (2010), Regional chemical diversity, crustal and mantle sources and evolution of central Andean Puna Plateau ignimbrites, *J. Volcanol. Geotherm. Res.*, *198*(1–2), 81–111, doi:10.1016/j.jvolgeores.2010.08.013.

Kellogg, J. N. and T. H. Dixon (1990), Central and South America GPS geodesy—CASA Uno, *Geophys. Res. Lett.*, *17*(3), 195–198, doi:10.1029/GL017i003p00195.

Kendrick, E., M. Bevis, R. Smalley Jr., and B. Brooks (2001), An integrated crustal velocity field for the central Andes, *Geochem. Geophys. Geosyst.*, *2*(11), 1066, doi:10.1029/2001GC000191.

Khazaradze, G., and J. Klotz (2003), Short- and long-term effects of GPS measured crustal deformation rates along the south central Andes, *J. Geophys. Res.*, *108*(B6), 2289, doi:10.1029/2002JB001879.

Klotz, J., and D. Lelgemann (1988), Present state of the central Andean GPS-traverse ANSA, GPS-Techniques Applied to Geodesy and Surveying, edited by E. Groten, and R. Strauß, Lect. Notes Earth Sci., 19, 427–436.

Lee, J., J. Garwood, D. F. Stockli, and J. Gosse (2009), Quaternary faulting in Queen Valley, California-Nevada: Implications for kinematics of fault-slip transfer in the eastern California shear zone-Walker Lane belt, *Geol. Soc. Am. Bull.*, *121*(3–4), 599–614, doi:10.1130/B26352.1.

Leffler, L., S. Stein, A. Mao, T. Dixon, M. A. Ellis, L. Ocola, and I. S. Sacks (1997), Constraints on present-day shortening rate across the central eastern Andes from GPS data, *Geophys. Res. Lett.*, *24*(9), 1031–1034, doi:10.1029/97GL00770.

Marquillas, R. A., C. del Papa, and I. F. Sabino (2005), Sedimentary aspects and paleoenvironmental evolution of a rift basin: Salta Group (Cretaceous–Paleogene), northwestern Argentina, *Int. J. Earth Sci.*,*94*, 94–113

Marrett, R., and R. W. Allmendinger (1992), Amount of extension on small faults—An example from the Viking Graben, *Geology*, *20*(1), 47–50.

Marrett, R., and S. H. Emerman (1992), The relations between faulting and mafic magmatism in the Altiplano Puna Plateau (central Andes), *Earth Planet. Sci. Lett.*, *112*(1–4), 53–59.

Marrett, R., and M. R. Strecker (2000), Response of intracontinental deformation in the central Andes to late Cenozoic reorganization of South American plate motions, *Tectonics*, *19*(3), 452–467.

Marrett, R. A., R. W. Allmendinger, R. N. Alonso, and R. E. Drake (1994), Late Cenozoic tectonic evolution of the Puna Plateau and adjacent foreland, northwestern Argentine Andes, *J. South Am. Earth Sci.*, *7*(2), 179-207.

McCaffrey, R., and J. Nabelek (1998), Role of oblique convergence in the active deformation of the Himalayas and southern Tibet Plateau, *Geology*, *26*(8), 691–694.

McGlashan, N., L. Brown, and S. Kay (2008), Crustal thickness in the central Andes from teleseismically recorded depth phase precursors, *Geophys. J. Int.*, *175*(3), 1013–1022, doi:10.1111/j.1365-246X.2008.03897.x.

McQuarrie, N. (2002), Initial plate geometry, shortening variations, and evolution of the Bolivian orocline, *Geology*, *30*(10), 867–870.

Mercier, J. L., M. Sebrier, A. Lavenu, J. Cabrera, O. Bellier, J.-F. Dumont, and J. Machrare (1992), Changes in the tectonic regime above a subduction zone of Andean Type: The Andes of Peru and Bolivia during the Pliocene-Pleistocene, *J. Geophys. Res.*, *97*(B8), 11,945–11,982, doi:10.1029/90JB02473.

Montero Lopez, M. C. M., F. D. Hongn, M. R. Strecker, R. Marrett, R. Seggiaro, and M. Sudo (2010), Late Miocene–early Pliocene onset of N-S extension along the southern margin of the Central Andean Puna Plateau: Evidence from magmatic, geochronological and structural observations, *Tectonophysics*, *494*(1–2), 48–63, doi:10.1016/j.tecto.2010.08.010.

Mpodozis, C., C. Arriagada, M. Basso, P. Roperch, P. Cobbold, and M. Reich (2005), Late mesozoic to paleogene stratigraphy of the Salar de Atacama Basin, Antofagasta, Northern Chile: Implications for the tectonic evolution of the central Andes, *Tectonophysics*, *399*(1–4), 125–154, doi:10.1016/j.tecto.2004.12.019.

Norabuena, E., L. Leffler-Griffin, A. L. Mao, T. Dixon, S. Stein, I. S. Sacks, L. Ocola, and M. Ellis (1998), Space geodetic observations of Nazca-South America convergence across the central Andes, *Science*, *279*, 358–362.

Oncken, O., D. Hindle, J. Kley, K. Elger, P. Victor, and K. Schemmann (2006), Deformation of the central Andean upper plate system: Facts, fiction, and constraints for plateau models, in The Andes: Active Subduction Orogeny, edited by O. Oncken, et al., pp. 3–27, Springer, Berlin.

Pardo-Casas, F., and P. Molnar (1987), Relative motion of the Nazca (Farallon) and South American plates since Late Cretaceous time, *Tectonics*, *6*(3), 233–248.

Petrinovic, I. A., U. Riller, and J. A. Brod (2005), The Negra Muerta Volcanic Complex, southern central Andes: Geochernical characteristics and magmatic evolution of an episodically active volcanic centre, *J. Volcanol. Geotherm. Res.*, *140*(4), 295–320.

Pysklywec, R. N., and A. R. Cruden (2004), Coupled crust-mantle dynamics and intraplate tectonics: Two-dimensional numerical and three-dimensional analogue modeling, *Geochem. Geophys. Geosyst.*, *5*, Q10003, doi:10.1029/2004GC000748.

Pysklywec, R. N., O. Gogus, J. Percival, A. R. Cruden, and C. Beaumont (2010), Insights from geodynamical modeling on possible fates of continental mantle lithosphere: Collision, removal, and overturn, *Can. J. Earth Sci.*, *47*(4), 541–563, doi:10.1139/E09-043.

Ramos, V. A. (2008), The basement of the central Andes: The Arequipa and related terranes, *Annu. Rev. Earth Planet. Sci.*, *36*, 289–324, doi:10.1146/annurev.earth.36.031207.124304.

Rey, P., O. Vanderhaeghe, and C. Teyssier (2001), Gravitational collapse of the continental crust: definition, regimes and modes, *Tectonophysics*, *342* (3–4), 435–449.

Richards, J. P., and M. Villeneuve (2002), Characteristics of late Cenozoic volcanism along the Archibarca lineament from Cerro Llullaillaco to Corrida de Cori, northwest Argentina, *J. Volcanol. Geotherm. Res.*, *116*, 161–200.

Riller, U., and O. Oncken (2003), Growth of the Central Andean Plateau by tectonic segmentation is controlled by the gradient in crustal shortening, *J. Geol.*, *111*(3), 367–384.

Riller, U., I. Petrinovic, J. Ramelow, M. Strecker, and O. Oncken (2001), Late Cenozoic tectonism, collapse caldera and plateau formation in the central Andes, *Earth Planet. Sci. Lett.*, *188*(3–4), 299–311.

Riller, U., A. R. Cruden, D. Boutelier, and C. E. Schrank (2012), The causes of sinuous crustal-scale deformation patterns in hot orogens: Evidence from scaled analogue experiments and the southern central Andes, *J. Struct. Geol.*, *37*, 65–74.

Risse, A., R. B. Trumbull, B. Coira, S. M. Kay, and P. van den Bogaard (2008), $^{40}Ar/^{39}Ar$ geochronology of mafic volcanism in the back-arc region of the southern Puna Plateau, Argentina, *J. South Am. Earth Sci.*, *26*(1), 1–15, doi:10.1016/j.jsames.2008.03.002.

Royden, L. H., B. C. Burchfiel, and R. D. van der Hilst (2008), The geological evolution of the Tibetan Plateau, *Science*, *321*, 1054–1058, doi:10.1126/science.1155371.

Santimano, T., and U. Riller (2012), Kinematics of Tertiary to Quaternary intracontinental deformation of upper crust in the Eastern Cordillera, southern central Andes, NW Argentina, *Tectonics*, *31*, TC4002, doi:10.1029/2011TC003068.

Schoenbohm, L. M., and M. R. Strecker (2009), Normal faulting along the southern margin of the Puna Plateau, northwest Argentina, *Tectonics*, *28*, TC5008, doi:10.1029/2008TC002341.

Schreiber, U., and K. Schwab (1991), Geochemistry of quaternary shoshonitic lavas related to the Calama-Olacapato-El Toro Lineament, NW Argentina, *J. South Am. Earth Sci.*, *4*(1–2), 73–85.

Schurr, B., A. Rietbrock, G. Asch, R. Kind, and O. Oncken (2006), Evidence for lithospheric detachment in the central Andes from local earthquake tomography, *Tectonophysics*, *415*(1–4), 203–223, doi:10.1016/j.tecto.2005.12.007.

Schoenbohm, L. M., B. Carrapa (2011), Evidence from the timing of contraction, extension, sedimentation and magmatism for small-scale lithospheric foundering in the Puna Plateau, NW Argentina, *American Geophysical Union*, Fall Meeting 2011

Simoes, M., J. P. Avouac, and Y.-G. Chen (2007), Slip rates on the Chelungpu and Chushiang thrust faults inferred from a deformed strath terrace along the Dungpuna river, west central Taiwan, *J. Geophys. Res.*, *112*, B03S10, doi:10.1029/2005JB004200.

Singer, B. S., R. P. Ackert, and H. Guillou (2004), $^{40}Ar/^{39}Ar$ and K-Ar chronology of Pleistocene glaciations in Patagonia, *Geol. Soc. Am. Bull.*, *116*(3–4), 434–450, doi:10.1130/B25177.1.

Somoza, R. (1998), Updated Nazca (Farallon) - South America relative motions during the last 40 My: implications for mountain building in the central Andean region, *J. South Am. Earth Sci.*, *11*(3), 211–215.

Spell, T. L., and I. McDougall (2003), Characterization and calibration of $^{40}Ar/^{39}Ar$ dating standards, *Chem. Geol.*, *198*(3–4), 189–211, doi:10.1016/S0009-2541(03)00005-6.

Tassara, A., H.-J. Götze, S. Schmidt, and R. Hackney (2006), Three-dimensional density model of the Nazca plate and the Andean continental margin, *J. Geophys. Res.*, *111*, B09404, doi:10.1029/2005JB003976.

Taylor, M. and G. Peltzer (2006), Current slip rates on conjugate strike-slip faults in central Tibet using synthetic aperture radar interferometry, *J. Geophys. Res.*, *111*, B12402, doi:10.1029/2005JB004014.

Taylor, M., A. Yin, F. J. Ryerson, P. Kapp, and L. Ding (2003), Conjugate strike-slip faulting along the Bangong-Nujiang suture zone accommodates coeval east-west extension and north-south shortening in the interior of the Tibetan Plateau, *Tectonics*, *22*(4), 1044, doi:10.1029/2002TC001361.

Whitman, D., B. L. Isacks, J. L. Chatelain, J. M. Chiu, and A. Perez (1992), Attenuation of high-frequency seismic waves beneath the Central Andean Plateau, *J. Geophys. Res.*, *97*(B13), 19,929–19,947.

Whitman, D., B. L. Isacks, and S. M. Kay (1996), Lithospheric structure and along-strike segmentation of the Central Andean Plateau: Seismic Q, magmatism, flexure, topography and tectonics, *Tectonophysics*, *259* (1–3), 29–40.

Yin, A., P. A. Kapp, M. A. Murphy, C. E. Manning, T. M. Harrison, M. Grove, D. Lin, X. G. Deng, and C. M. Wu (1999), Significant late Neogene east-west extension in northern Tibet, *Geology*, *27*(9), 787–790.

Yuan, X., S. V. Sobolev, and R. Kind (2002), Moho topography in the central Andes and its geodynamic implications, *Earth Planet. Sci. Lett.*, *199* (3–4), 389–402, doi:10.1016/S0012-821X(02)00589-7.